Journal of Materials Chemistry C

Interfacial Doping of Semiconducting Polymers with Phenothiazine-based Polymeric Ionic Liquids

Journal:	*Journal of Materials Chemistry C*
Manuscript ID	TC-ART-09-2023-003176.R1
Article Type:	Paper
Date Submitted by the Author:	29-Sep-2023
Complete List of Authors:	Oh, Saejin; University of California Santa Barbara, Nguyen, Phong; University of California Santa Barbara, Tran, Thi; University of California Santa Barbara, Chemistry and Biochemistry DeStefano, Audra; University of California Santa Barbara, Chemical Engineering Tagami, Kan; University of California, Department of Chemistry and Biochemistry Yuan, Dafei; Hunan University, College of Materials Science and Engineering Nikolaev, Andrei; University of California-Santa Barbara, Dept. of Chemical Engineering Condarcure, Marcus; University of California, Department of Chemical Engineering Han, Songi; University of California Santa Barbara Read de Alaniz, Javier; University of California Santa Barbara, Chemistry Chabinyc, Michael; University of California Santa Barbara, Materials

Interfacial Doping of Semiconducting Polymers with Phenothiazine-based Polymeric Ionic Liquids

Saejin Oh,[a] Phong H. Nguyen,[b] Thi M. Tran,[a] Audra J. DeStefano,[b] Kan Tagami,[a] Dafei Yuan[c], Andrei Nikolaev,[a] Marcus Condarcure,[b] Songi Han,[a,b] Javier Read de Alaniz,[a] and Michael L. Chabinyc[d*]*

[a]Department of Chemistry and Biochemistry, [b]Department of Chemical Engineering, [c]Mitsubishi Center for Advanced Materials, University of California, Santa Barbara, CA, 93106–5050, USA, [d]Materials Department, University of California, Santa Barbara, California 93106, United States

KEYWORDS Polymeric Ionic Liquids, Redox-Active, Semiconducting Polymers, Interfacial Doping, Charge Transfer

Abstract. Molecular *p*-type dopants, widely used to electrically dope semiconducting polymers, are challenging to design because of the requirements for their redox potentials. Redox-active dopants with radical cations present a strategy to achieve effective doping and to increase their synthetic versatility. A *p*-type dopant from a phenothiazine radical-cation bearing polymeric ionic liquid (PIL) with an associated bis(trifluoromethanesulfonyl)azanide ($(CF_3SO_2)_2N^-$, $TFSI^-$) counterion was investigated. The structure of the polymeric dopant limits mass diffusion into solid polymer films allowing charge transfer to occur only at interfaces. Electron transfer between the phenothiazine radical cation and model semiconducting polymers was found to be similar in both the small molecule and pendant attached polymer. The kinetics of charge transfer upon forming bilayers with the PIL and poly(3-hexylthiophene) (P3HT) was investigated and the limiting factor was found to be mass diffusion of the charge balancing $TFSI^-$ counterion in the solid state. The electrical conductivity and microstructural changes in P3HT film were consistent with the doping levels expected based on the radical cation fraction in the polymeric dopant. This redox-active PIL allows facile charge generation and broadens the choice of *p*-type dopants for semiconducting polymers.

Introduction.

Semiconducting polymers are attractive materials for electronic applications due to their ease of processability enabling additive manufacturing.[1–4] The doping level of these materials is important for their electrical conductivity and control of the occupancy of electronic states necessary for improving the performance of organic electronic devices.[5–7] Doping of semiconducting polymers is usually achieved through the introduction of either *p*- or *n*-type small-molecular dopants.[5,8] With strategically matched frontier electronic levels between the dopant molecule and the semiconducting polymer, electrons can be transferred from the donor to the acceptor to form charge carriers (electrons or holes). For electronic devices, it is important to understand how to control not only the total concentration of dopants, but also their spatial profile in thin films.

While doping can be performed in either a solution or solid state, the choice of processing route is critical for controlling the morphologies of the semiconducting polymer which ultimately dictates the electrical performance. Solution-state doping is an effective route to induce charge carriers, but the aggregates formed by electrostatic interactions of the donor-acceptor pairs can interrupt the formation of ordered microstructures during solidification of conjugated polymer films.[9–11] Alternatively, solid-state doping approaches where dopants are added to a solid film can maintain their morphology providing effective charge transport pathways.[12,13] Dopants that are easily sublimed can be used to dope semiconducting polymers from the vapor phase. For instance, 2,3,5,6-tetrafluoro-7,7,8,8-tetracyanoquinodimethane (F_4TCNQ)[12–14] and nitrosonium hexafluorophosphate ($NOPF_6$)[15] can be readily volatilized and subsequently diffuse into

semiconducting polymer films. The preservation of the microstructure of conjugated polymer thin films during vapor phase doping can lead to significant increases in conductivity relative to doping in solution.[16] An alternative method for solid-state doping is a direct exposure of the semiconducting polymer thin films to a solution of dopant. Practically, this is done by dipping the solid semiconducting polymer layers into a dopant solution or by spin-casting the solution on the semiconducting polymer.[5,11] This method allows for control over the degree of doping by controlling the concentration of the dopant solutions.[6,17,18]

The sequential doping process is effective, but restricted by i) limited dopant choices, ii) uncertainties on the dopant penetration depth, iii) difficulty in precise control over doping levels, and iv) requirement for orthogonal solvents. In particular, the choice of the dopants is limited to strong dopants such as F_4TCNQ (electron affinity, EA=5.2 eV), tris(4-bromophenyl)ammoniumyl hexachloroantimonate (Magic Blue, EA of radical cation form=5.8 eV), or $NOPF_6$ (EA of $NO^{\bullet+}$ =6.5 eV) (Table S1); note that for the radical cations we define the EA based on their reduction potential to their neutral form as referenced to the vacuum level. While they work as powerful *p*-type dopants for semiconducting polymers, their volatility and strong oxidizing capability make them challenging to precisely control the extent of doping or the stability of doped polymers. The high reactivity of strong acids can also achieve oxidative doping very quickly. This could overly oxidize a donor polymer to generate radical dications, or could form undesired side products due to high reactivity.[19] For example, strong oxidants such as Magic Blue can form dimers and suffer from side reactions with long term storage.[20] Additionally, nitrosonium in $NOPF_6$ can be easily hydrolyzed to generate nitrous acid, and thus lose its ability to oxidize semiconducting polymers, which make it challenging to control the degree of doping reproducibly.[19,21] Ideally, a *p*-type

dopant that addresses these limitations listed above would help improve control over doping and expand the versatility of this approach to improve the performance of organic electronic devices.

Doping semiconducting polymers can also be achieved with other classes of redox-active species that can donate or accept electrons.[22–24] –For example, molecular radical cations are promising dopants for semiconducting polymers, but there have been relatively few studies to examine their behavior. The radical cation Magic Blue is a very strong oxidant that can dope polymers with a wide range of IEs to form charge carriers.[25–27] Another radical cation, 2,2′,7,7′-tetrakis(N,N-di-p-methoxyphenylamine)- 9,9′-spirobifluorene (Spiro-OMeTAD) with a bis(trifluoromethanesulfonyl)azanide ($(CF_3SO_2)_2N^-$, $TFSI^-$) counterion, is a weaker oxidizing agent (EA of the radical cation form is ~ 5.3 eV with a summary of IE and EA shown in Table S1) that has been used successfully to dope small molecules and semiconducting polymers.[28]

While radical cations provide a route to tune the oxidation potential of dopants, modification of known materials can be limited synthetically. To increase the versatility of synthesis here we examine phenothiazine (PTZ), which forms stable radical cations when oxidized and has appropriate energetics to control electron transfer with organic semiconductors.[29] PTZ has been widely introduced in batteries as a redox-active molecules and was demonstrated to generate robust and stable radical cations.[30–32] In our previous work, we have synthesized polymers with sidechain-attached PTZ units that are N-substituted with 2-(2-ethoxyethoxy)ethoxy)ethyl (EE) groups referred to as (pPTZ-EE).[29] The EE groups served to lower the glass transition temperature, T_g, of (pPTZ-EE) and to improve the solubility of the polymer. We demonstrated the use of PTZ radical cation pendants as redox-active low-T_g and charge-conducting polymeric ionic liquids (PILs), i.e. charged polymers incorporating units akin to common ionic liquids.[29] The radical

cations present in the PTZ-containing polymer chain could be adjusted by a controlled oxidation reaction with the amount of $TFSI^-$ counter anions, which resulted in tunable electrical conductivity with radical/$TFSI^-$ loading. Herein, we describe the use of redox-active PTZ-containing polymers to boost the electrical conductivity of poly(3-hexylthiophene) (P3HT). We find here that an oxidized form of a PTZ-containing polymeric dopant can induce efficient electron transfer between a PTZ radical cation ($PTZ^{\bullet+}$) with a P3HT semiconducting donor. Importantly, the use of a polymeric dopant instead of a small-molecule dopant provides precise control over the amount of dopant introduced into the P3HT by controlling both the radical cation concentrations and constraining diffusion into the P3HT film. To our knowledge, there are very few demonstrations of introducing either a polymeric or redox-active polymer as a surface-limited dopant and the approach differs from electrolyte gating where doping effectively occurs by injection from electrodes.[33,34] Lastly, the stability of the neutral redox-active PIL layer provides additional stability to the doped semiconducting polymer film.

Results and Discussion.

Design of redox-active PILs as p-type dopants.

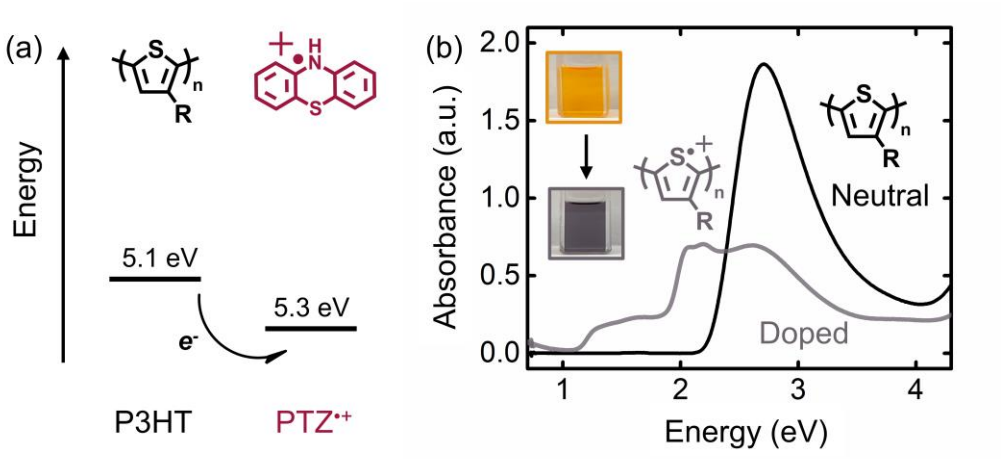

Figure 1. (a) Ionization energy diagram of P3HT and PTZ. (b) UV-vis-NIR spectra of pristine (black trace) and doped (gray trace) P3HT solutions with 35.2% $PTZ^{\bullet+}$:$TFSI^-$ small molecules. Inset figures indicate color changes from pristine to doped P3HT with $PTZ^{\bullet+}$:$TFSI^-$.

As indicated in **Fig. 1a**, $PTZ^{\bullet+}$ has EA of 5.3 eV,[35–37] which is ≈0.2 eV lower than the IE of P3HT. The relatively small energy difference makes $PTZ^{\bullet+}$ a mild oxidant for P3HT and is comparable to F_4TCNQ. As expected from the energy difference, mixing the radical cation salt $PTZ^{\bullet+}$:$TFSI^-$ and P3HT in a solution induced integer charge transfer evidenced by bleaching of the neutral absorbance of P3HT (~1-2 eV) and appearance of the polaron absorptions (~0.5 and 1.5 eV) along with spectral shifts indicating aggregation of doped P3HT[12,38–40] (**Fig. 1b**). Given the observation of doping by $PTZ^{\bullet+}$, it suggested a route to use the synthetic versatility of PTZ to form polymeric dopants that are challenging to form using many conventional molecular dopants.[41–43]

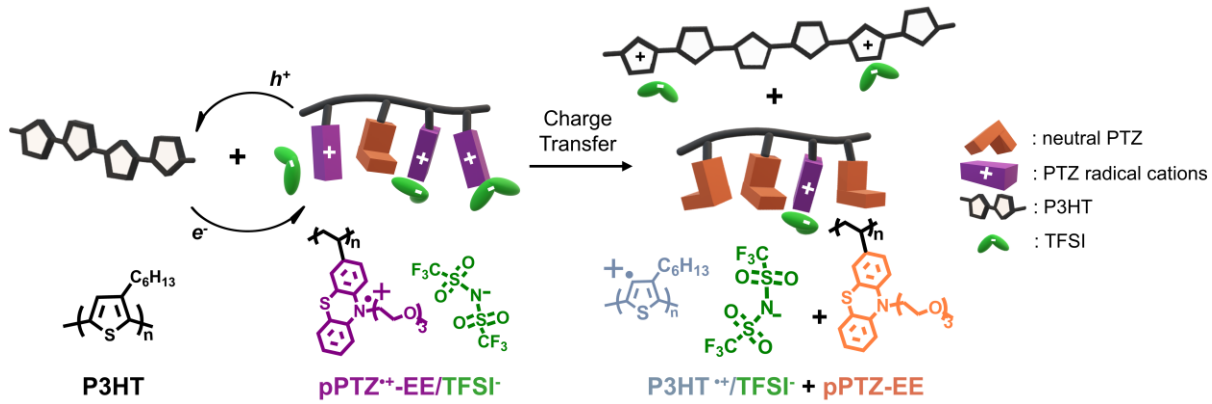

Scheme 1. Overall schematic to induce surface doping of the P3HT layer with $pPTZ\text{-}EE^{\bullet+}$:$TFSI^-$ leading to formation of $P3HT^+$ charge balanced by $TFSI^-$ and neutral PTZ-EE units.

Polymeric dopants provide the ability to study doping processes at interfaces of semiconducting polymers and on the kinetics of doping in the bulk. Doping of semiconducting polymers by sequential casting of molecular dopants or ion exchange methods can help to preserve

the microstructure of the polymer that enable efficient charge conducting pathways.[5,13,15,44] For most sequential doping strategies, however, small molecular dopants are directly cast onto conjugated polymer films from a solvent making it unclear i) if charge transfer happens only at the polymer top interface, or in the bulk after diffusion of the dopant, and ii) if diffusion of charged species, i.e. the counterion, affects doping and charge conducting behavior. Tethering the dopants to the backbone of a polymer can dramatically slow any possible interdiffusion and allow charge transfer at a surface only providing a means to examine the factors leading to effective doping.[44–46]

We designed a $PTZ^{\bullet+}$-based polymer for sequential doping as shown in **Scheme 1**. Charge transfer between the pPTZ-$EE^{\bullet+}$ and the semiconducting polymer occurs at the interface as the dopant solution contacts the film, followed by migration of $TFSI^-$ ion migration for charge neutrality (**Scheme 2**). We tested this process with P3HT which undergoes charge transfer in solution with $PTZ^{\bullet+}$. A clear color change from deep to faint purple was observed upon sequential spin-coating of pPTZ-$EE^{\bullet+}$:$TFSI^-$ onto a P3HT film. Highly doped P3HT film is nearly colorless in the visible region suggesting that the *p*-type doping mostly occurred at the interface as expected with limited $TFSI^-$ ion penetration depth. This result is in contrast with other sequential doping with small molecules, where ions can diffuse into the bulk film.[6] In contrast, when the diketopyrrolo-[3,4-c]pyrrole-based polymer, DPP-DTT, with IE ~ 5.4 eV, was used as the semiconductor,[27] no significant doping was observed (Fig. S1) due to the energetic barrier for electron transfer. As expected, matching the energy level of the semiconductor and radical cation is critical for successful doping by electron transfer.

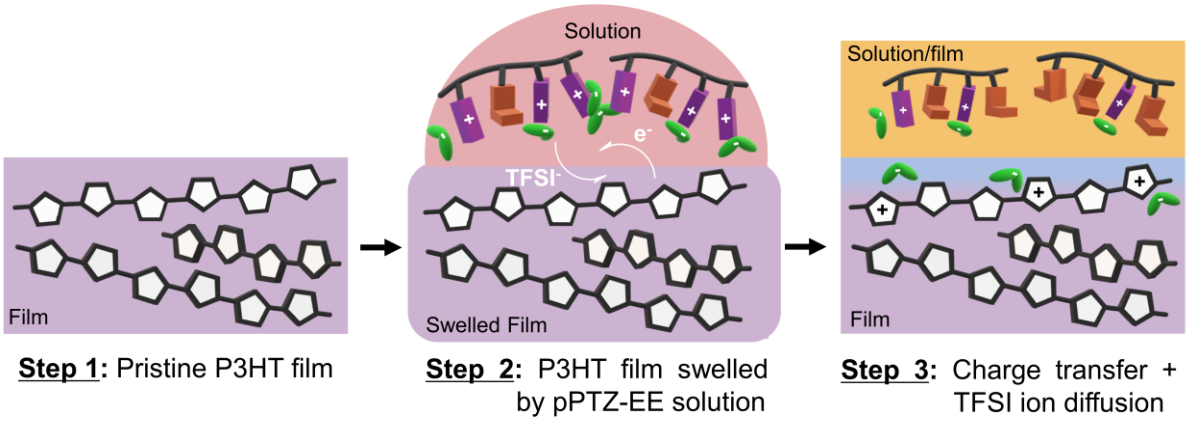

Scheme 2. Overall sample preparation and charge transfer process of interfacial doping of P3HT thin films with pPTZ-EE$^{\bullet+}$:TFSI$^-$.

Solvent controls the doping depth of P3HT. The partial bleaching of the optical absorbance of neutral P3HT observed in the P3HT/pPTZ-EE$^{\bullet+}$:TFSI$^-$ bilayer films, suggests that the charge transfer occurs initially only near the P3HT/pPTZ-EE$^{\bullet+}$:TFSI$^-$ interface. The optical absorption of the neutral form of P3HT remained bleached even after removing the pPTZ-EE$^{\bullet+}$:TFSI$^-$ layer with a DCM wash, indicating that TFSI$^-$ transferred to the P3HT layer to maintain neutrality by compensating the charge carrier. We therefore carried out depth profiling to determine how far the TFSI$^-$ diffused into the P3HT film after removal of pPTZ-EE$^{\bullet+}$:TFSI$^-$ (**Fig. 2**). The observed continuous decay in the F1s signal shows that TFSI$^-$ diffuses into the P3HT layer up to ≈13 nm. We examined the UV-vis-NIR spectra and the depth profile after 0.5 hr to 24 hrs (Fig. S2 and S3), from depositing the pPTZ- EE$^{\bullet+}$:TFSI$^-$ layer with no significant change in the optical absorption spectrum or the penetration depth of TFSI$^-$. These observations suggest that TFSI$^-$ only penetrates the P3HT layer in a very short timeframe, presumably during the spin-coating process.

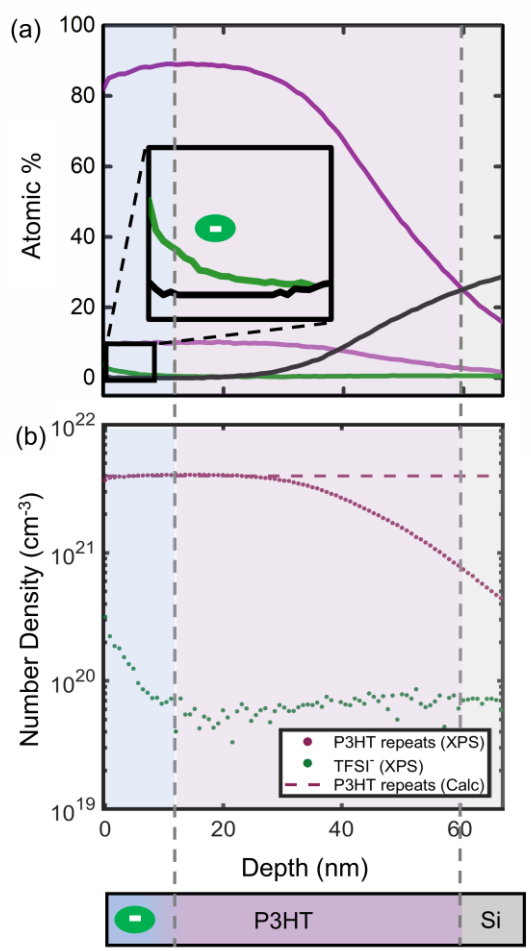

Fig 2. (a) Depth profile of surface doped 60 nm P3HT layer with 11.5% $PTZ^{\bullet+}$:$TFSI^-$. The top pPTZ-$EE^{\bullet+}$:$TFSI^-$ layer was spun-cast on the P3HT layer and the bilayer was left for 24 hours, then the top layer was removed by DCM wash prior to the measurements. The crossover point of C1s and Si2p was set to be the interface of the P3HT film and the Si substrate. Green, darker/lighter purple, and black traces correspond to F1s, C1s, S2s, and Si2p, respectively. (Inset) Magnified F1s spectra near the surface of the doped P3HT film. (b) $TFSI^-$ number density plot over depth of the film. The relative number of $TFSI^-$ ions were extracted by assuming one polaron (and thus one $TFSI^-$) is delocalized throughout ten 3HT repeat units.

To understand the depth of the doping process, we have to consider the factors that influence charge transfer between the two polymers. We do not expect that pPTZ-$EE^{\bullet+}$ can interdiffuse into the P3HT film rapidly because of its high molecular weight, but the small molecule counterion $TFSI^-$ will diffuse into P3HT to balance the charge carrier formed by electron

transfer. The choice of solvent, which causes swelling, should affect the counterion diffusion into the P3HT film.[8,44] The solubility of the donor polymer in sequential coating solvent also affects the swelling and can lower its glass transition temperature promoting diffusion of molecular species. Here, dichloromethane (DCM) was chosen as a solvent for pPTZ-EE$^{\bullet+}$:TFSI$^-$ that did not readily dissolve P3HT. P3HT has both crystalline and amorphous regions in solid state and upon swelling, we expect that the amorphous regions will be swelled and induce volume expansion.[47] Moreover, the dielectric constant of solvent also affects the Coulombic interaction of the cations/anions in dopant solutions with higher dielectric constants favoring dissociation of the counterion from pPTZ-EE$^{\bullet+}$:TFSI$^-$. The dielectric constant of DCM is ≈9 whereas that of P3HT is ≈2 so the ion pair is more likely to dissociate in solvent than in the solid state. We therefore posit that charge transfer occurs between the pPTZ-EE$^{\bullet+}$ and P3HT chains at the solution-film interface followed by diffusion of TFSI$^-$ ions into the P3HT film along with intercalation into P3HT crystallites.

The penetration depth of doping into P3HT thin films should also depend on the diffusion of the charge carrier formed and the TFSI$^-$ counterion away from the interface. Recently, our group has reported the kinetics of doping and diffusion of Brønsted acid doping from solution of P3HT using HTFSI.[18] The coupled P3HT$^{\bullet+}$:TFSI$^-$ pairs showed a relatively slow diffusion coefficient of ~1.0 nm^2 min^{-1} based on reaction-diffusion modeling. Although methanol was used as the solvent for the acid doping process, which swells P3HT differently than DCM, we can use the diffusion coefficient as a rough estimate here. The counterion penetration observed here from the depth profiling (~13 nm) on the timescale (~1 min) is deeper than the expected depth from data on the diffusion of P3HT$^{\bullet+}$:TFSI$^-$. This difference is likely due to swelling by DCM that could increase the diffusion constant. We note that the roughness of the P3HT thin film (±5 nm) could lead to

deeper apparent ion penetration depth than the estimate from XPS depth profiling. Further diffusion in bulk P3HT film is very limited once the film is dried. Previously, study showed that $TFSI^-$ counterion has very restricted diffusion above the observed doping depth even with prolonged thermal annealing at elevated temperature.[18] This could be ascribed to the increased modulus and shift in T_g observed for doped conjugated polymers, and thus limiting the mobility of the counterions from the doped surfaces.[48,49]

Interfacial doping induces polaron formation and higher electrical conductivity. For P3HT/pPTZ-$EE^{\bullet+}$ bilayers, UV-Vis-NIR revealed that the bilayers showed both absorption peaks from neutral pPTZ-EE and pPTZ-$EE^{\bullet+}$:$TFSI^-$ (**Fig. 3a**). In addition to their original absorption, a decrease in neutral peak transition at ~2.0-2.5 eV was observed due to successful charge transfer, with the appearance of integer charge transfer transition at ~1.5 eV and polaron transition at ~0.5 eV. To investigate the relationship between the % $PTZ^{\bullet+}$:$TFSI^-$ present in the PIL and the resulting P3HT doping, PILs with lower fractions of $PTZ^{\bullet+}$ were used to form bilayers. The percentage of $PTZ^{\bullet+}$:$TFSI^-$ units in the polymer was tuned by adjusting the amount of oxidant added to the neutral pPTZ-EE, and extracting the % converted to $PTZ^{\bullet+}$ by spin quantification from EPR. The resulting percentage represents the overall fraction of $PTZ^{\bullet+}$:$TFSI^-$ groups present in the polymer chain. When lower % $PTZ^{\bullet+}$:$TFSI^-$ concentrations were used for doping, a subsequent decreasing trend in doping was observed (Table S2). Higher $PTZ^{\bullet+}$ fractions in pPTZ-$EE^{\bullet+}$:$TFSI^-$ layer generally induced stronger charge transfer and polaron absorptions, followed by sequential decrease in neutral P3HT transition (**Fig. 3b**). The relative absorption of neutral (~2.3 eV) and polaron (~0.5 eV) peaks were used to extract the actual $TFSI^-$ counterion concentration assuming 1 counterion per carrier with 60 nm thick films.[5,13] Note that these ratios are averaged % dopant loadings throughout the entire film thickness, while the doping occurs at the P3HT/pPTZ-$EE^{\bullet+}$:$TFSI^-$ bilayer

interfaces only as shown in the depth profiles. The actual number of $PTZ^{\bullet+}$ used for each sequential P3HT layer doping was higher than the number of 3HT unit present in P3HT layer (up to ~2 equivalence for 11.5% $PTZ^{\bullet+}$:$TFSI^-$, see details in calculation in Supplementary Information). We ascribe the low actual dopant loading into P3HT layer due to limited surface exposure of pPTZ-$EE^{\bullet+}$:$TFSI^-$ to the bottom layer prior to spin coating, and significant amount of the pPTZ-$EE^{\bullet+}$:$TFSI^-$ solution is lost during spin coating. Nevertheless, the increasing trend of doping with higher % $PTZ^{\bullet+}$:$TFSI^-$ loading is clearly observed by the increased population of polarons and $TFSI^-$ counterions. Due to the relatively slow $TFSI^-$ diffusion, doping is expected to occur only at the P3HT/pPTZ-$EE^{\bullet+}$:$TFSI^-$ interfaces regardless of % $PTZ^{\bullet+}$:$TFSI^-$ present in the pPTZ-$EE^{\bullet+}$:$TFSI^-$ layer.

From the absorption spectra of doped P3HT thin films, the changes in the 0-0:0-1 ratio provide important insight in understanding which population of the P3HT crystallites are preferentially doped at each stage. The changes in the P3HT thin film absorption spectra was observed *in-situ* with sufficiently dilute pPTZ-$EE^{\bullet+}$:$TFSI^-$ solution (3HT:$TFSI^-$ = 1: 0.8), in order to monitor the gradual change in vibronic features at 2.0-2.4 eV (Fig S5). As the P3HT thin film is doped by prolonged soaking in a pPTZ-$EE^{\bullet+}$:$TFSI^-$ solution, a higher 0-0:0-1 ratio was observed indicating more crystalline regions (H aggregate) are preferentially consumed at the early stage of doping which is consistent with our other studies with P3HT thin film doping with $TFSI^-$ counterions.[50–52] The concentrated pPTZ-$EE^{\bullet+}$:$TFSI^-$ solutions that were used for doping showed a faster doping process, with fast loss of vibronic features at 2.0-2.4 eV. These spectral features indicate that both H and J-type aggregates were oxidized due to higher $TFSI^-$ loading.[50,52] Thus, the combined observation with vibronic peaks indicate that the overall doping process is expected

to occur at the more crystalline region at the early stages of doping, followed by amorphous regions of the P3HT thin film.

The electrical conductivity and polaron absorbance both increased with the percentage of dopant in pPTZ-EE$^{\bullet+}$:TFSI$^-$ (**Fig. 3c**). Both UV-vis-NIR absorption and conductivity were preserved after removing the pPTZ-EE$^{\bullet+}$:TFSI$^-$ layer (Fig. S6 and S7). These results are consistent with the TFSI$^-$ counterion insertion depth of ≈13 nm from depth profiling by XPS. The expected number density of TFSI$^-$ ion estimated in **Fig. 2b** assumes that one polaron is delocalized throughout ten 3HT repeat units, and the resulting number density of TFSI$^-$ ion at doped P3HT film surface was expected to be ~10^{20} cm^3 (assuming equivalence number of charge carriers and TFSI$^-$ counterions). Compared to similar P3HT doping studies with TFSI$^-$ ions, a similar order of magnitude of carrier concentration and electrical conductivity at relatively low doping regime was observed.[50,52] Note that the electrical conductivity measurements were performed by measuring the whole depth of the doped and undoped P3HT thin film, thus the extracted conductivity values in Fig. 3c could be relatively lower when compared to other reported studies on P3HT with similar carrier concentrations.[12,13]

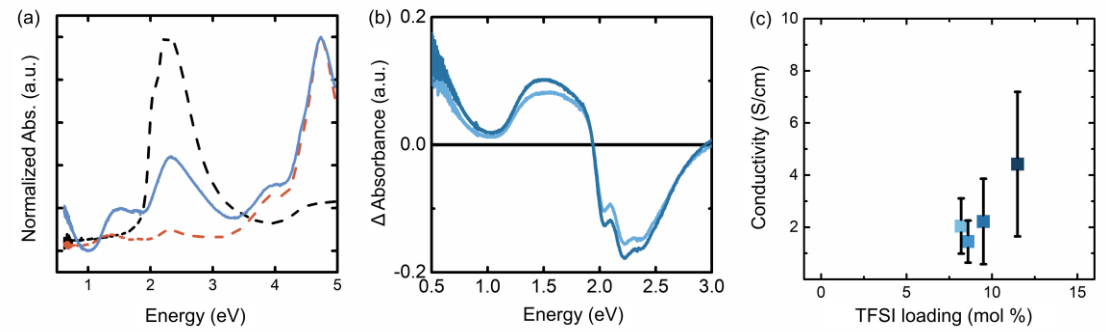

Fig 3. (a) UV-vis-NIR spectra of (black, dashed) pristine P3HT, (red, dashed) 11.5% PTZ$^{\bullet+}$:TFSI$^-$ loaded PIL, and (blue, solid) 11.5% PTZ$^{\bullet+}$:TFSI$^-$ loaded PIL/P3HT bilayer. (b) Subtracted absorbance of PIL/P3HT bilayers that were subtracted with neutral P3HT absorption spectra.

(black) Pristine P3HT and (lighter and darker blue) P3HT/pPTZ-EE$^{\bullet+}$:TFSI$^-$ bilayers with 8.2 and 11.5% PTZ$^{\bullet+}$:TFSI$^-$ loadings, respectively. (c) Electrical conductivity of interfacial doped P3HT films with pPTZ-EE$^{\bullet+}$:TFSI$^-$ with various dopant loading. The degree of % PTZ$^{\bullet+}$:TFSI$^-$ used for bilayers was indicated from lighter to darker blue labels. Both UV-vis-NIR and conductivity measurements were done with 60 nm P3HT thin films that were sequentially casted with 5 mg/mL pPTZ-EE$^{\bullet+}$:TFSI$^-$ in DCM.

As discussed earlier, bilayers were formed with sufficient ion concentrations (~ 2 equivalents relative to 3HT units in the entire film thickness) and the major doping process occurred while the bilayers were formed. There were no obvious changes in conductivity of bilayers at longer timescales up to two months (Fig. S7) indicating that the doping occurs rapidly initially and then is essentially fixed. The charge transfer could have occurred as soon as the P3HT film was exposed to the pPTZ-EE$^{\bullet+}$:TFSI$^-$ solution prior to spin casting (less than a few seconds), or during the casting process (> 30 sec) while solvent is evaporating. To access a more rapid timescale, we dipped a P3HT thin films in a pPTZ-EE$^{\bullet+}$:TFSI$^-$ solution with the same concentration used for spin-casting (Fig. S8) and found that the electrical conductivity plateaued within ≈5 seconds of exposure time. Both solution dipping and spin-casting methods showed comparable conductivity increase and no further increase in conductivity was observed after prolonged dipping time. This observation indicates that with 60 nm thick P3HT film and the concentrated pPTZ-EE$^{\bullet+}$:TFSI$^-$ solution, charge transfer occurs in a very short time frame at the interface. Both the excessive TFSI$^-$ concentration used for doping and prolonged swelling time do not appear to substantially change the distance of ion diffusion.

In addition to the spectroscopic and electrical measurements, thicker P3HT films (200 nm) were also studied with grazing incidence wide angle x-ray scattering (GIWAXS) to further understand the ion insertion with interfacial doping. From the X-ray scattering images, clear shifts

in the q_{xy} and q_z were observed (**Fig. 4a**) with doping. More specifically, a consistent increase in the (100) alkyl spacing from 16.0 to 17.5 Å was observed with higher dopant loading (**Fig. 4b**) indicating that the $TFSI^-$ ion resides in the alkyl chains. As more dopants are introduced into the P3HT film, it showed a simultaneous decrease in (010) π-π stacking distance from 3.79 to 3.66 Å (**Fig. 4c**), indicating the stronger interchain interaction induced by electronic doping. The observed changes in alkyl spacing and π-π stacking distances are consistent with studies of doping in P3HT.[12,13,15] The sharp transition in these structural changes have been observed at critical carrier concentration, in between ~10^{20} and $10^{21}$$cm^3$.[50] This steep shift is consistent to the observed trend in the alkyl spacing and π-π stacking distances in Fig. 4b and the level of doping observed in UV-Vis spectra of thinner samples (Fig. 3); we note that the alkyl spacing here is below the value of the most heavily doped samples in literature of 18.5 Å. While the exact carrier concentration is difficult to extract, the estimated carrier density based on the shift in the crystalline domains is expected to be around ~10^{20} and 10^{21} cm^3 and is consistent with the estimated number density of $TFSI^-$ ions discussed above, which was ~10^{20} cm^3.

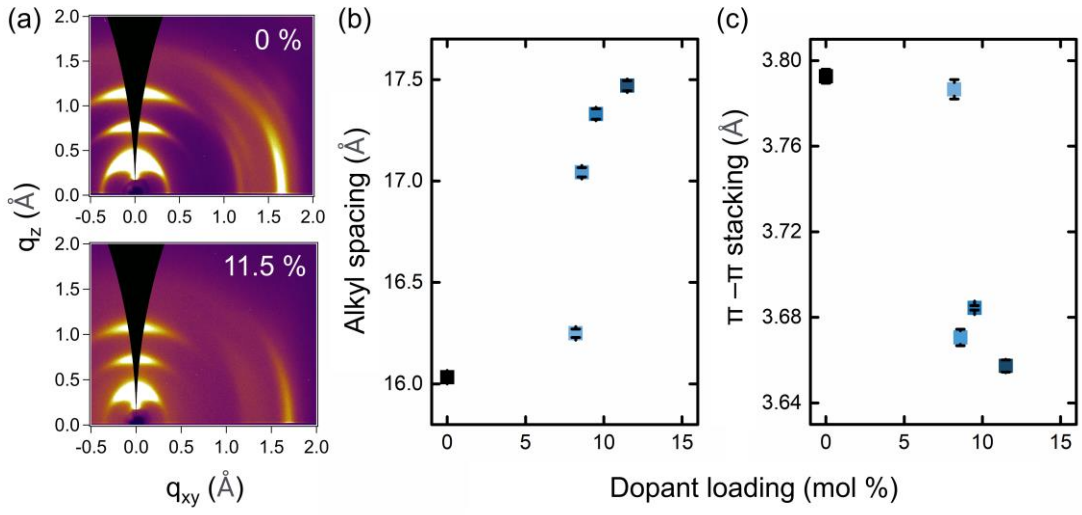

Fig 4. (a) GIWAXS scattering images of pristine (0%) and doped P3HT film with 11.5% $pPTZ^{\bullet+}$:$TFSI^-$. Extracted (b) alkyl spacing and (c) π-π stacking distances of sequentially doped 200 nm P3HT films with pPTZ-$EE^{\bullet+}$:$TFSI^-$ with various dopant loading. The average distances of alkyl spacing and π-π stacking are reported from the measurement of bulk films with incidence angle of 0.13°.

Conclusion

In summary, pPTZ-$EE^{\bullet+}$/$TFSI^-$ was introduced as the new *p*-type dopant for semiconducting polymer films. The polymeric structure of the dopant layer limited charge transfer to the interface of the semiconducting polymer with solvent swelling leading to limited counter anion penetration into the bulk. Precise energy matching between the two materials was proved to be the critical consideration to induce the facile charge transfer between the two layers with P3HT films having effective charge transfer. The extent of oxidation of P3HT could be finely controlled with the percentage of oxidized groups in pPTZ-$EE^{\bullet+}$:$TFSI^-$. Given that the most significant increase in the conductivity was observed right after the spin-coating, or within a very short timeframe of the dopant solution exposure, the kinetics of doping are fast on the timescale of typical processing methods. While P3HT films were successfully oxidized by pPTZ-$EE^{\bullet+}$:$TFSI^-$, full control of the interfacial profile of doping requires further investigation of the diffusion kinetics of counterions as a function of solvent and polymer. The polymeric dopant ensures that the charge transfer occurs at the dopant/P3HT interface and the depth of doping into the P3HT layer depends on the diffusion of $P3HT^{\bullet+}$:$TFSI^-$ pairs through the bulk. The use of bulkier counterions or a polymeric counterion could provide further control of the depth of doping. At the same time, various PTZ derivatives allow facile synthesis to modify the energetics of the surface-limited doping process.

Supporting Information

The Supporting Information is available free of charge on the RSC website.

AUTHOR INFORMATION

Corresponding Author

* Michael L. Chabinyc – Materials Department, University of California, Santa Barbara, California 93106, United States

Email: mchabinyc@engineering.ucsb.edu

*Javier Read de Alaniz – Department of Chemistry and Biochemistry, University of California, Santa Barbara, California 93106, United States

Email: javier@chem.ucsb.edu

Author Contributions

Oh, S., Chabinyc, M., and Read de Alaniz, J. led the project, designed experiments, and wrote the manuscript. Oh, S. carried out optical spectroscopy, electrical measurements, and data analysis. Nguyen. P. performed XPS, GIWAXS, and assisted with data analysis. Tran. T. synthesized PTZ monomer and polymer. DeStefano, A. and Tagami, K. performed EPR measurements for radical spin counts. Yuan, D. assisted with DPP-DTT doping. Nikolaev, A. and Condarcure, M. assisted

with the sample preparations for materials characterizations. Han, S. provided helpful suggestions on EPR experiments. All authors have given approval to the final version of the manuscript.

Notes

The authors declare no competing financial interest.

ACKNOWLEDGMENT

The research reported here was primarily supported by the National Science Foundation (NSF) through the Materials Research Science and Engineering Center at UC Santa Barbara, DMR–2308708 (IRG-1). This research made use the Stanford Synchrotron Radiation Lightsource, SLAC National Accelerator Laboratory, is supported by the U.S. Department of Energy, Office of Science, Office of Basic Energy Sciences under Contract No. DE-AC02-76SF00515. A portion of this work was performed in the UCSB Nanofabrication Facility, an open access laboratory. P. H. N. gratefully acknowledges support from the National Science Foundation Graduate Research Fellowship Program under grant no. 2139319. Any opinions, findings, and conclusions or recommendations expressed in this material are those of the authors and do not necessarily reflect the views of the National Science Foundation.

REFERENCES

1 M. K. Akbari, S. Zhuiykov, S. U. Zschieschang, H. Klauk and U. Zschieschang, *J Mater Chem C Mater*, 2019, **7**, 5522–5533.

2 H. Sirringhaus, *Advanced Materials*, 2014, **26**, 1319–1335.

3 C. Wang, H. Dong, W. Hu, Y. Liu and D. Zhu, *Chem Rev*, 2011, **112**, 2208–2267.

4 S. Logothetidis, *Materials Science and Engineering: B*, 2008, **152**, 96–104.

5 I. E. Jacobs, E. W. Aasen, J. L. Oliveira, T. N. Fonseca, J. D. Roehling, J. Li, G. Zhang, M. P. Augustine, M. Mascal and A. J. Moulé, *J Mater Chem C Mater*, 2016, **4**, 3454–3466.

6 V. A. Kolesov, C. Fuentes-Hernandez, W.-F. Chou, N. Aizawa, F. A. Larrain, M. Wang, A. Perrotta, S. Choi, S. Graham, G. C. Bazan, T.-Q. Nguyen, S. R. Marder and B. Kippelen, *Nature Materials 2017 16:4*, 2016, **16**, 474–480.

7 Y. Yamashita, J. Tsurumi, M. Ohno, R. Fujimoto, S. Kumagai, T. Kurosawa, T. Okamoto, J. Takeya and S. Watanabe, *Nature*, 2019, **572**, 634–638.

8 I. E. Jacobs, A. J. Moulé *Advanced Materials*, 2017, **29**, 1703063.

9 F. M. McFarland, L. R. Bonnette, E. A. Acres and S. Guo, *J Mater Chem C Mater*, 2017, **5**, 5764.

10 A. M. Glaudell, J. E. Cochran, S. N. Patel, M. L. Chabinyc, A. M. Glaudell, S. N. Patel, M. L. Chabinyc and J. E. Cochran, *Adv Energy Mater*, 2015, **5**, 1401072.

11 D. T. Scholes, S. A. Hawks, P. Y. Yee, H. Wu, J. R. Lindemuth, S. H. Tolbert and B. J. Schwartz, *Journal of Physical Chemistry Letters*, 2015, **6**, 4786–4793.

12 E. Lim, A. M. Glaudell, R. Miller and M. L. Chabinyc, *Adv Electron Mater*, 2019, **5**, 1800915.

13 E. Lim, K. A. Peterson, G. M. Su and M. L. Chabinyc, *Chemistry of Materials*, 2018, **30**, 998–1010.

14 E. M. Thomas, E. C. Davidson, R. Katsumata, R. A. Segalman and M. L. Chabinyc, *ACS Macro Lett*, 2018, **7**, 1492–1497.

15 E. M. Thomas, K. A. Peterson, A. H. Balzer, D. Rawlings, N. Stingelin, R. A. Segalman and M. L. Chabinyc, *Adv Electron Mater*, 2020, **6**, 2000595.

16 K. Kang, S. Watanabe, K. Broch, A. Sepe, A. Brown, I. Nasrallah, M. Nikolka, Z. Fei, M. Heeney, D. Matsumoto, K. Marumoto, H. Tanaka, S. I. Kuroda and H. Sirringhaus, *Nature Materials 2016 15:8*, 2016, **15**, 896–902.

17 S. Watanabe, R. Hakamatani, K. Yaegashi, Y. Yamashita, H. Nozawa, M. Sasaki, S. Kumagai, T. Okamoto, C. G. Tang, L.-L. Chua, P. K. H. Ho and J. Takeya, *Advanced Science*, 2021, **8**, 2002065.

18 P. H. Nguyen, M. B. Schmithorst, T. E. Mates, R. A. Segalman and M. L. Chabinyc, *J Mater Chem C Mater*, 2023, **11**, 7462–7470.

19 N. G. Connelly and W. E. Geiger, *Chem Rev*, 1996, **96**, 877–910.

20 M. R. Talipov, M. M. Hossain, A. Boddeda, K. Thakur and R. Rathore, *Org Biomol Chem*, 2016, **14**, 2961–2968.

21 J. K. Kochi, *Acc Chem Res*, 1992, **25**, 39–47.

22 J. Kim, J. H. Kim and K. Ariga, *Joule*, 2017, **1**, 739–768.

23 S. Muench, A. Wild, C. Friebe, B. Häupler, T. Janoschka and U. S. Schubert, *Chem Rev*, 2016, 116, 9438–9484.

24 M. Burgess, J. S. Moore and J. Rodríguez-López, *Acc Chem Res*, 2016, **49**, 2649–2657.

25 D. Kiefer, R. Kroon, A. I. Hofmann, H. Sun, X. Liu, A. Giovannitti, D. Stegerer, A. Cano, J. Hynynen, L. Yu, Y. Zhang, D. Nai, T. F. Harrelson, M. Sommer, A. J. Moulé, M. Kemerink, S. R. Marder, I. McCulloch, M. Fahlman, S. Fabiano and C. Müller, *Nature Materials 2019 18:2*, 2019, **18**, 149–155.

26 E. Järsvall, T. Biskup, Y. Zhang, R. Kroon, S. Barlow, S. R. Marder and C. Müller, *Chemistry of Materials*, 2022, **34**, 5673–5679.

27 A. I. Hofmann, R. Kroon, S. Zokaei, E. Järsvall, C. Malacrida, S. Ludwigs, T. Biskup and C. Müller, *Adv Electron Mater*, 2020, **6**, 2000249.

28 M. Goel, M. Siegert, G. Krauss, J. Mohanraj, A. Hochgesang, D. C. Heinrich, M. Fried, J. Pflaum and M. Thelakkat, *Advanced Materials*, 2020, **32**, 2003596.

29 S. Oh, A. Nikolaev, K. Tagami, T. Tran, D. Lee, S. Mukherjee, R. A. Segalman, S. Han, J. Read De Alaniz and M. L. Chabinyc, *ACS Appl Mater Interfaces*, 2021, **13**, 5319–5326.

30 J. A. Kowalski, M. D. Casselman, A. P. Kaur, J. D. Milshtein, C. F. Elliott, S. Modekrutti, N. H. Attanayake, N. Zhang, S. R. Parkin, C. Risko, F. R. Brushett and S. A. Odom, *J Mater Chem A Mater*, 2017, **5**, 24371–24379.

31 J. D. Milshtein, A. P. Kaur, M. D. Casselman, J. A. Kowalski, S. Modekrutti, P. L. Zhang, N. Harsha Attanayake, C. F. Elliott, S. R. Parkin, C. Risko, F. R. Brushett and S. A. Odom, *Energy Environ Sci*, 2016, **9**, 3531–3543.

32 S. A. Odom, S. Ergun, P. P. Poudel and S. R. Parkin, *Energy Environ Sci*, 2014, **7**, 760–767.

33 K. Xu, H. Sun, T.-P. Ruoko, G. Wang, R. Kroon, N. B. Kolhe, Y. Puttisong, X. Liu, D. Fazzi, K. Shibata, C.-Y. Yang, N. Sun, G. Persson, A. B. Yankovich, E. Olsson, H. Yoshida, W. M. Chen, M. Fahlman, M. Kemerink, S. A. Jenekhe, C. Müller, M. Berggren and S. Fabiano, *Nature Materials 2020 19:7*, 2020, **19**, 738–744.

34 A. Legrand and S. Furukawa, *Nature Materials 2020 19:7*, 2020, **19**, 702–704.

35 K. A. Narayana, M. D. Casselman, C. F. Elliott, S. Ergun, S. R. Parkin, C. Risko and S. A. Odom, *ChemPhysChem*, 2015, **16**, 1179–1189.

36 M. Li, Z. Rhodes, J. R. Cabrera-Pardo and S. D. Minteer, *Sustain Energy Fuels*, 2020, **4**, 4370–4389.

37 N. H. Attanayake, J. A. Kowalski, K. V. Greco, M. D. Casselman, J. D. Milshtein, S. J. Chapman, S. R. Parkin, F. R. Brushett and S. A. Odom, *Chemistry of Materials*, 2019, **31**, 4353–4363.

38 K. A. Peterson and M. L. Chabinyc, *J Mater Chem C Mater*, 2022, **10**, 6287–6295.

39 M. J. Nowak, D. Spiege, S. Hotta, A. J. Heeger and P. A. Pincus, *Macromolecules*, 1989, **22**, 2917–2926.

40 M. Arvind, C. E. Tait, M. Guerrini, J. Krumland, A. M. Valencia, C. Cocchi, A. E. Mansour, N. Koch, S. Barlow, S. R. Marder, J. Behrends and D. Neher, *Journal of Physical Chemistry B*, 2020, **124**, 7694–7708.

41 H. Gilman and D. A. Shirley, *J Am Chem Soc*, 1944, **66**, 888–893.

42 H. Tian, X. Yang, R. Chen, Y. Pan, L. Li, A. Hagfeldt and L. Sun, *Chemical Communications*, 2007, 3741–3743.

43 D. F. Houston, E. B. Kester and F. DeEds, *J Am Chem Soc*, 1949, **71**, 3816–3818.

44 I. E. Jacobs, Y. Lin, Y. Huang, X. Ren, D. Simatos, C. Chen, D. Tjhe, M. Statz, L. Lai, P. A. Finn, W. G. Neal, G. D'Avino, V. Lemaur, S. Fratini, D. Beljonne, J. Strzalka, C. B. Nielsen, S. Barlow, S. R. Marder, I. McCulloch and H. Sirringhaus, *Advanced Materials*, 2021, 2102988.

45 G. K. Mor, D. Jones, T. P. Le, Z. Shang, P. J. Weathers, M. K. B Woltermann, K. Vakhshouri, B. P. Williams, S. A. Tohran, T. Saito, R. Verduzco, A. Salleo, M. A. Hickner, E. D. Gomez, G. K. Mor, T. P. Le, P. J. Weathers, M. K. B Woltermann, K. Vakhshouri, B. P. Williams, S. A. Tohran, E. D. Gomez, D. Jones, T. Saito and M. A. Hickner, *Adv Energy Mater*, 2014, **4**, 1400439.

46 W. L. Seah, C. G. Tang, R. Q. Png, V. Keerthi, C. Zhao, H. Guo, J. G. Yang, M. Zhou, P. K. H. Ho and L. L. Chua, *Adv Funct Mater*, 2017, **27**, 1606291.

47 J. C. Aguirre, S. A. Hawks, A. S. Ferreira, P. Yee, S. Subramaniyan, S. A. Jenekhe, S. H. Tolbert and B. J. Schwartz, *Adv Energy Mater*, 2015, **5**, 1402020.

48 S. Zokaei, D. Kim, E. Järsvall, A. M. Fenton, A. R. Weisen, S. Hultmark, P. H. Nguyen, A. M. Matheson, A. Lund, R. Kroon, M. L. Chabinyc, E. D. Gomez, I. Zozoulenko and C. Müller, *Mater Horiz*, 2022, **9**, 433–443.

49 J. Hynynen, D. Kiefer, L. Yu, R. Kroon, R. Munir, A. Amassian, M. Kemerink and C. Müller, *Macromolecules*, 2017, **50**, 8140–8148.

50 E. M. Thomas, M. A. Brady, H. Nakayama, B. C. Popere, R. A. Segalman, M. L. Chabinyc, E. M. Thomas, H. Nakayama, R. A. Segalman, M. L. Chabinyc, M. A. Brady and B. C. Popere, *Adv Funct Mater*, 2018, **28**, 1803687.

51 B. C. Popere, G. E. Sanoja, E. M. Thomas, N. S. Schauser, S. D. Jones, J. M. Bartels, M. E. Helgeson, M. L. Chabinyc and R. A. Segalman, *J Mater Chem C Mater*, 2018, **6**, 8762–8769.

52 D. Rawlings, E. M. Thomas, R. A. Segalman and M. L. Chabinyc, *Chemistry of Materials*, 2019, **31**, 8820–8829.